Transients Behavior of a Fixed-Speed Grid-Connected Wind Farm

Ahmadreza Tabesh, *Student Member, IEEE*, Reza Iravani, *Fellow, IEEE*

***Abstract*— This paper investigates the transient behavior of a grid-connected wind farm perturbed with electrical and mechanical disturbances. A grid-connected wind farm system study is introduced based on radial network configuration for this investigation. Several case studies are presented to investigate the transients of a wind farm following an electrical disturbance, *e.g.* a three-phase short circuit, and a mechanical disturbance, *e.g.* a wind gust. Case studies are developed based on time-domain simulation using EMTDC/PSCAD software tool. It has been shown that mechanical disturbances mainly effect on voltage quality. However, electrical disturbances impact on voltage quality and excite torsional modes of the wind turbine-generator shaft system. The paper also deals with the impacts of steady-state operating point, network resonance modes and the network stiffness on the shaft system torsional behavior, and compares the effect of multi-mass and single-mass modelling on voltage quality during an electrical disturbance. Influence of network stiffness on torsional oscillation and voltage quality following an electrical and mechanical disturbance are also investigated.**

***Index Terms*—Wind farm transients, torsional dynamics, grid-connected fixed-speed wind farm, time-domain simulations, wind turbine modelling.**

I. Introduction

Rapid developments in wind power technologies indicate proliferation of wind farms in the electric power systems [1]. This necessitates investigation and understanding of electromagnetic transients and dynamic phenomena due to the interactions between a wind farm and corresponding host utility system due to various faults and their subsequent switching incidents.

Based on a time-domain simulation model of a fixed-speed wind farm in the PSCAD/EMTDC environment, this paper investigates impacts of electrical and mechanical disturbances on the transient behavior of the wind turbine-generator units. The wind farm is represented by two equivalent wind units and also the impact of unequal loading conditions of the wind units are investigated. The studies conclude that:
(i) Electrical disturbances, *e.g.* a fault and its subsequent fault clearing incidents, can results in noticeable shaft torsional dynamics of the wind units, and also the voltage quality at the point of common coupling of the wind farm.
(ii) Mechanical disturbance, *e.g.* a wind gust, primarily impacts the voltage at the point of common coupling and do not effect the shaft torques of the wind turbine-generator units.

The authors are with the Department of Electrical and Computer Engineering, University of Toronto, Toronto, ON M5S 3G4, Canada.
E-mails: a.tabesh@utoronto.ca, iravani@ecf.utoronto.ca

Presented at the International Conference on Power Systems Transients (IPST'05) in Montreal, Canada on June 19-23, 2005
Paper No. IPST05-068

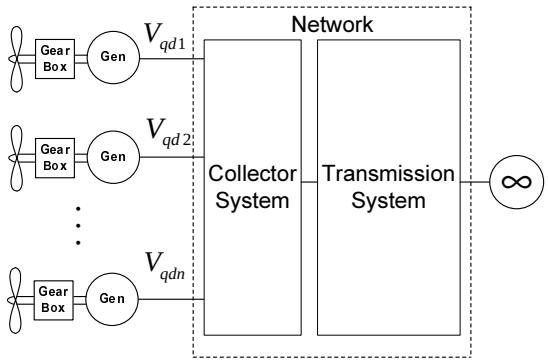

Fig. 1. Grid-connected wind farm configuration

II. Grid-Connected Wind Farm

Figure 1 shows a grid-connected wind farm configuration. Each generator unit is a fixed-speed induction machine unit. The wind turbine-generators are connected to the network through a collector system. The collector system can be considered as a part of network. The infinite bus represents that part of the power system that can be considered as a fixed-frequency constant-magnitude voltage source.

III. Mathematical Model of the System

A. Wind turbine

A wind turbine encompasses rotor blades, hub, and pitch control system. Pitch control system is an electrical/hydrulic servomechanism that changes the pitch angle using the generator output power as a feedback. The pitch control servomechanism has slow dynamics in comparison to the electromechanical dynamics. Thus, the pitch control dynamic is neglected in power system transient analysis [2], [3]. For power system studies, the rotor blades and hub dynamics have a subordinate role [2], [4]. Thus, the wind turbine aerodynamic is modelled with an algebraic equation as given by [1]

$$P_R = \frac{1}{2}\rho\pi R^2 C_p(\lambda,\beta)V_w^3 \tag{1}$$

where P_R is the rotor power, V_w is the wind speed and $C_p(\lambda,\beta)$ is the characteristic power coefficient. $C_p(\lambda,\beta)$ is a function of tip speed ratio λ, and the pitch angle β. ρ and R are the air density and blade radius, respectively. The tip speed ratio λ is defined by

$$\lambda = \frac{\omega_R R}{V_w} \tag{2}$$

where ω_R is the angular speed of rotor blades.

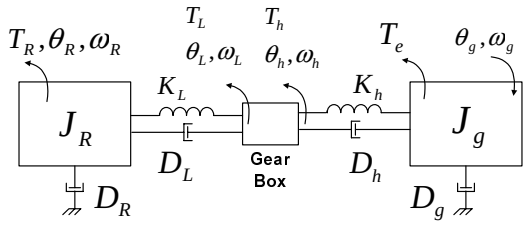

Fig. 2. Shaft system of a wind turbine-generator unit

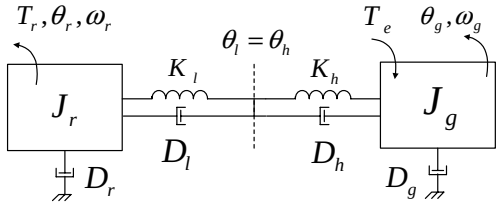

Fig. 3. The transferred shaft system to the high-speed side

B. Shaft System

Figure 2 shows shaft system of a wind turbine-generator. The shaft system includes low- and high-speed shafts and gear-box. Figure 3 shows the mass-spring-damper representation of the shaft system. In Fig. 3 the low-speed shaft system is transferred to the high-speed side of gear-box where

J_r is the transferred rotor blade and the hub total mass;
J_g is the generator rotor mass;
$K_l,\ K_h$ are shafts spring constant;
$D_l,\ D_h$ are shafts damping constant;
$D_r,\ D_g$ are shafts windage damping constant.

The mass of rotating part of the gear-box is ignored in comparison to those of the rotor blade and generator rotor mass. The mass-spring-damper model of the shaft system is a linear system. Hence, the dynamic of the shaft system can be expressed by

$$\theta = G_m(s)T \tag{3}$$

where

$$\theta_j = [\theta_{r_j}\ \ \theta_{g_j}]^T$$
$$T_j = [T_{r_j}\ \ T_{e_j}]^T \tag{4}$$

$G_m(s)$ is a 2×2 transfer-function matrix. The entries of $G_m(s)$ is obtained by solving the dynamical equation of the system of Fig. 3.

C. Generator

The set of voltage equations for the jth induction machine of the Fig. 1, in the network synchronously rotating reference frame, is given by [5]

$$M_j(p)i_j^e = v_j^e \tag{5}$$

where

$$v_j^e = [v_{qs_j}^e\ \ v_{ds_j}^e\ \ v_{0s_j}^e\ \ v_{qr_j}^e\ \ v_{dr_j}^e\ \ v_{0r_j}^e]^T$$
$$i_j^e = [i_{qs_j}^e\ \ i_{ds_j}^e\ \ i_{0s_j}^e\ \ i_{qr_j}^e\ \ i_{dr_j}^e\ \ i_{0r_j}^e]^T$$

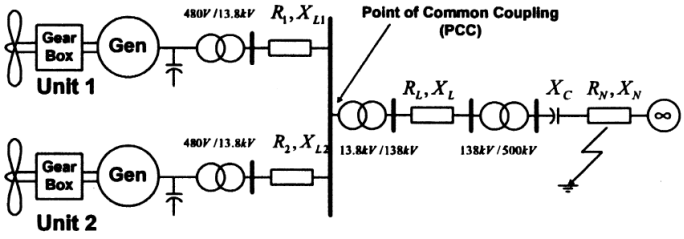

Fig. 4. Single-diagram of the study system

Superscript "e" indicates that the equations are written in the synchronously rotating reference frame. "p" represents the $\frac{d}{dt}$ operator, $M_j(p)$ elements are given in Appendix I. The air-gap torque for the induction machine, T_e, is [5]

$$T_{e_j} = \frac{3}{2}\frac{P}{2}M(i_{qs}^e i_{dr}^{'e} - i_{ds}^e i'e_{qr}) \tag{6}$$

where P is the number of machine poles and M is the machine mutual inductance. Notations of machine related resistance and inductance are adopted from [5].

D. Network

The wind turbine-generator sets interact through the network. For the frequency range of 1 to 50/60 Hz the radial network including the collector system is modelled as a multi-port circuit using lumped, linear, RLC components. The dynamic of the linear network, based on a set of ordinary linear differential equations, are embedded within the overall model of the system.

IV. Study System

Figure 1 shows a schematic diagram of the study system. The system is composed of a wind farm which is connected through its collector system to a radial network. The wind farm is composed of 80 identical wind turbine-generator units. Each unit is a fixed-speed, squirrel-cage induction machine rated at 330-kW and 480-V. The three-blade wind turbine is connected to the generator through a gear-box. Induction machine and mechanical parameters of the rotating system are given in Appendix II. Each machine is connected through a 400-kW, 480-V/13.8-kV transformer to the collector system.

The collector is interfaced to the network through a 38.4-MW, 13.8-kV/69-kV transformer. The 138-kV line is equipped with fixed series capacitors. The rest of the network is represented by an equivalent source with the short circuit capacity of 764.5-MVA and $X_\infty/R_\infty = 7$. Parameter of the collector system and the network are also given in Appendix II.

Figure 4 shows a single-line diagram representation of the study system. The wind farm, including the collector, is represented by two equivalent wind turbine-generator. Each equivalent unit represents 40 unison units which are operating at the same conditions.

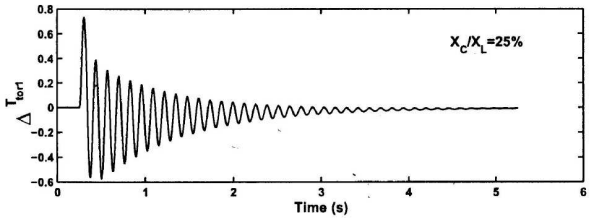

Fig. 5. Torsional torque of Unit 1 following an electrical disturbance, CASE 1

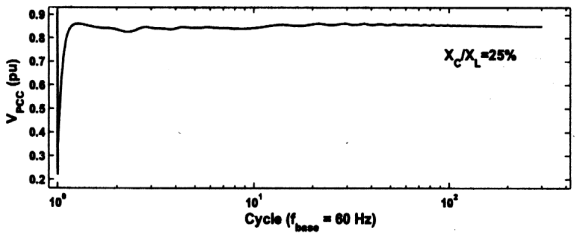

Fig. 6. Per unitized RMS value of the voltage at PCC, CASE 1

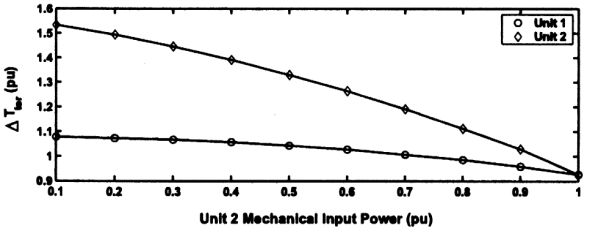

Fig. 7. Effects of non-uniform wind distribution on torsional torque dynamic, CASE 1

V. Case Studies

A. CASE 1

This case study investigates the impact of an electrical disturbance on torsional dynamics and voltage at the point of common coupling (V_{PCC}), Fig. 4. The electrical disturbance is a temporary, 3-cycle, three-phase to ground fault at the middle of the 138-kV line. Effects of non-uniform wind speed distribution on torsional dynamics of wind farm units are also investigated.

Initially, the system operates at a steady-state condition and identical wind speed for all units. Thus, the wind farm units are operating under identical conditions and the wind farm delivers 14.79-MW at $pf = 0.95$ (lagging) to the network. The compensation level of the series capacitor is adjusted to be 25% ($X_C/X_L = 25\%$). Then, the system is subjected to the electrical disturbance which is three-phase to ground fault at the middle of the 138-kV line. Figure 5 shows the torsional torque due to the electrical disturbance. Figure 6 depicts RMS value of V_{PCC} during and after the fault occurs. The Figs. 5 and 6 conclude that electrical disturbance excites torsional torque and impacts the voltage at the point of common coupling.

Figure 7 compares the maximum change in torsional torque and impacts the voltage at the point of common coupling.

Figure 7 compares the maximum change in torsional torques of the shafts of Unit 1 and Unit 2 of the system of Fig. 4 under different operating conditions. The mechanical input power of Unit 1 is kept constant at the rated power while the input power of Unit 2 is varied from 0.1 pu to 1 pu in steps of 0.1 pu. At each operating condition, the system is subjected the above described three-phase short circuit. Figure 7 shows that the unit that operates at the lower power, experiences significantly higher level of torsional stresses due to the electrical disturbance.

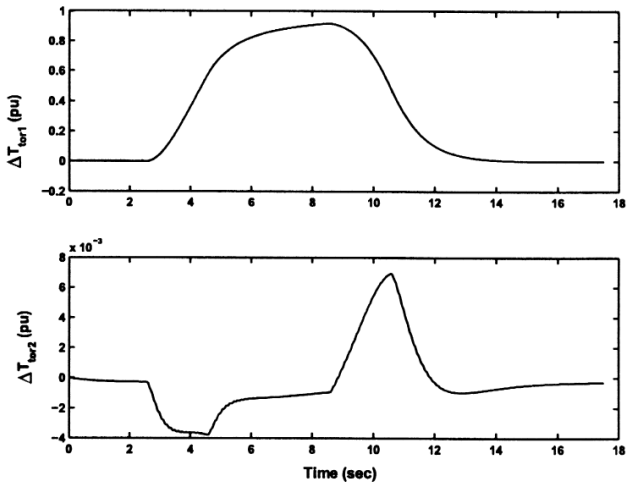

Fig. 8. Torsional torque oscillations following a mechanical disturbance, CASE 2

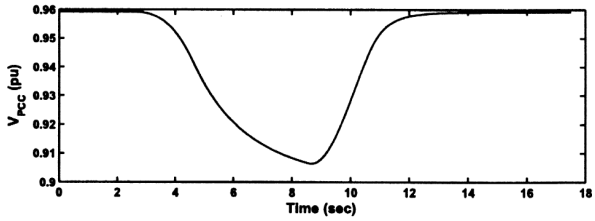

Fig. 9. RMS value of the voltage at PCC, CASE 2

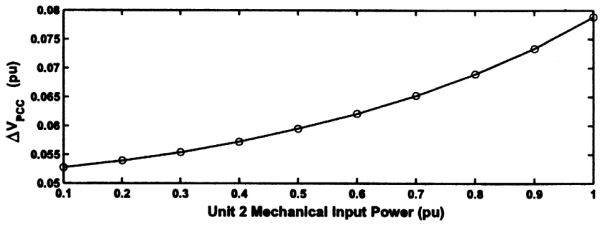

Fig. 10. Impact of operating point on V_{PCC} due to the mechanical disturbance, CASE 2

B. CASE 2

This case study deals with the impact of a mechanical disturbance on the torque dynamics and voltage at the point of common coupling. The first unit of Fig. 4 is operating at 50% of the rated power and the second one is operating at the rated power. Then, a wind gust signal is applied to the first unit as a mechanical disturbance. The wind gust is modelled by a trapezoidal changes in the input power to the first unit, with the magnitude of 1 per unit and the duration of 10 seconds. Figures 8 and 9 show changes in the torques and V_{PCC} RMS-value following the mechanical disturbance, does not significantly excite the turbine-generator torsional modes. This is expected since mechanical disturbances are low-frequency inputs.

To investigate the impacts of the steady-state operating point

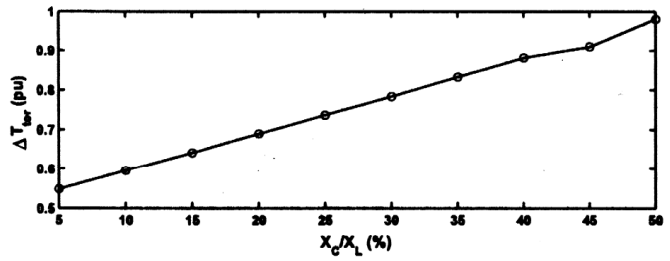

Fig. 11. Impact of network resonance frequency on maximum change in torsional torque following the electrical disturbance, CASE 3

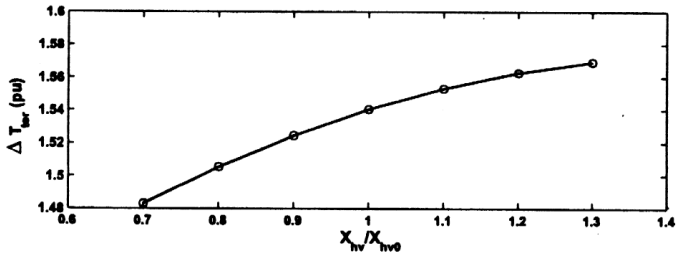

Fig. 12. Effects of network stiffness on torsional torques, CASE 4

on the system transient dynamics due to a mechanical disturbance, the input power of the second equivalent unit of the Fig. 4 is varied between 10% to 100% of the rated power and the disturbance is applied to the system. Figure 10 depicts the RMS-value of V_{PCC} in per unit with respect to different operating points. Figure 10 shows that the voltage drop due to the disturbance decreases as the generated power increases.

C. CASE 3

This case study investigates the effect of electrical network resonance on the turbine-generator torsional modes. The equivalent wind-turbine units are operating at the rated power under identical wind conditions. An electrical disturbance, identical to that of CASE 1, is applied to the network to excite the torsional dynamics.

Figure 11 depicts the changes in the maximum torsional torque when the compensation level X_C/X_L is varied between 5% to 50%, where X_C is the capacitor reactance and X_L is the line reactance including transformers' reactances, Fig. 4. Figure 11 concludes that torsional oscillation increases when the compensation level increases.

D. CASE 4

This case study considers the impact of network stiffness on the torsional dynamics and V_{PCC} of the gird-connected wind farm. The system of Fig. 4 initially operates at the rated power under identical wind conditions for both units. However, the electrical stiffness of the network is changed by changing the high voltage line reactance, X_{hv}, in the range of 0.7 to 1.3 of its nominal value, X_{hv0}. The X_C quantity is re-adjusted with respect to X_{hv} such that X_C/X_L remains constant to merely observe the effect of stiffness.

Figure 12 shows changes in the maximum torsional torque with respect to the X_{hv}/X_{hv0} when an electrical disturbance,

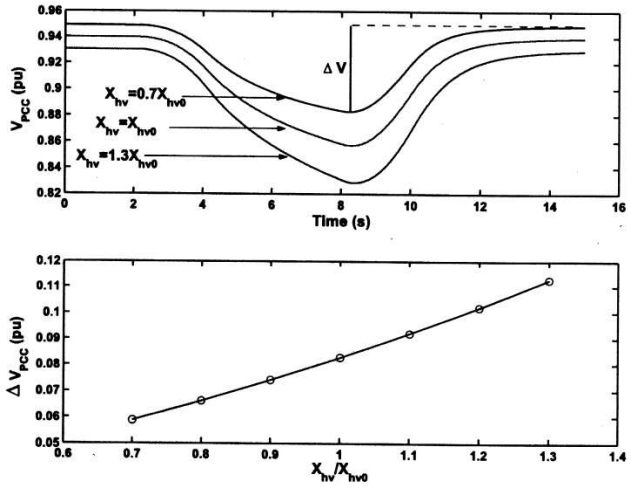

Fig. 13. Effects of network stiffness on V_{PCC}, CASE 4

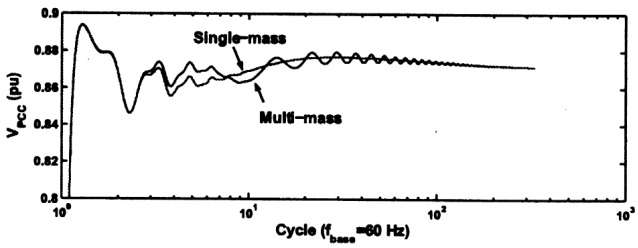

Fig. 14. V_{PCC} for single- and multi-mass wind turbine models following an electrical disturbance, CASE 5

the same as that of CASE 1, is applied to the system. Figure 12 conveys that the change in maximum torsional torque increases as the stiffness of the system decreases.

Figure 13 depicts the variations in RMS value of the voltage at PCC with respect to X_{hv}/X_{hv0}, when a mechanical disturbance, the same as that of CASE 2, is applied to the system. Figure 13 shows that the PCC voltage drop increases as the system stiffness decreases (X_{hv}/X_{hv0} increases).

E. CASE 5

This case study deals with the impact of turbine-generator mechanical model on electrical transient results. In the previous case studies the system of Fig. 4 was modelled as a two masses shaft system. In CASE 5, the shaft system is represented as a single, rigid mass. Thus, the torsional phenomenon is eliminated from the system study results. The compensation level in the system of Fig. 4 is set to $X_C/X_L = 35\%$ and an electrical fault, the same as that of CASE 1, is applied to the system. The RMS value of the voltage at the PCC is shown in Fig. 14. For the sake of comparison, the PCC voltage based on multi-mass shaft model is also plotted in Fig. 14. Comparison of the two voltage waveforms shows that the impact of torsional dynamics on the PCC voltage is noticeable and simplifying the mechanical model may results in inaccurate prediction of voltage after transient [6].

VI. Summary and Conclusion

The paper deals with the transients of a fixed-speed grid-connected wind farm. The wind farm is connected to a radial,

series-compensated network through a radial collector. Several case studies are developed and simulated to investigate the transient behavior of the system. The studies conclude that:

- Since the wind energy units of a wind farm are coupled through a network, there exist an interaction among the wind turbine-generator units when a disturbance occurs.
- An electrical disturbance excites torsional dynamic modes of the wind turbine-generator system and also impacts the quality at the wind farm PCC. However, mechanical disturbances mainly impact on voltage and do not excite torsional dynamics.
- The network resonance frequencies which are directly related to the series compensation level (X_C/X_L) impact the torsional torque amplitudes subsequent to an electrical disturbance.
- Non-identical units or non-identical operating conditions results in different transients behavior of wind units.
- The network stiffness directly effects the voltage quality at the point of common coupling following a disturbance.
- Using simplified single-mass model for a wind turbine unit can not provide accurate transient behavior of the system.

VII. Appendix I: Matrix $M_j(p)$ in (5)

The non-zero elements of $M_j(p)$ are

$$\begin{aligned}
&M_{j_{11}} = M_{j_{22}} = r_s + \tfrac{p}{\omega_b} X_{ss} \\
&M_{j_{44}} = M_{j_{55}} = r_s + \tfrac{p}{\omega_b} X'_{rr} \\
&M_{j_{33}} = r_s + \tfrac{p}{\omega_b} X_{ls} \\
&M_{j_{66}} = r_s + \tfrac{p}{\omega_b} X_{ls} \\
&M_{j_{14}} = M_{j_{25}} = M_{j_{41}} = M_{j_{52}} = \tfrac{p}{\omega_b} X_M \\
&M_{j_{12}} = -M_{j_{21}} = \tfrac{\omega}{\omega_b} X_{ss} \\
&M_{j_{15}} = -M_{j_{24}} = \tfrac{\omega}{\omega_b} X_M \\
&M_{j_{42}} = -M_{j_{51}} = \tfrac{\omega-\omega_r}{\omega_b} X_M \\
&M_{j_{45}} = -M_{j_{54}} = \tfrac{\omega-\omega_r}{\omega_b} X'_{rr}
\end{aligned}$$

where

$$\begin{aligned}
X_{ss} &= X_{ls} + X_M \\
X'_{rr} &= X'_{lr} + X_M
\end{aligned}$$

and X_{ls}, X'_{lr}, and X_M are machine reactances defined in [5].

VIII. Appendix II: Study System Data

A. Per Unit Base Values:

$S_{b_{3\phi}} = 100\ MVA$	$V_{b_{lv}} = 13.8\ kV$	$V_{b_{mv}} = 138\ kV$
$V_{b_{hv}} = 500\ kV$	$V_{b_{gen}} = 480\ V$	$\omega_b = 2\pi \times 60\ rad/s$

B. Network Parameter

$R_1 = 0.0006\ pu$	$X_{L_1} = 0.5004\ pu$
$R_2 = 0.0006\ pu$	$X_{L_2} = 0.5004\ pu$
$R_L = 0.1649\ pu$	$X_L = 0.7828\ pu$
$R_N = 0.0046\ pu$	$X_N = 0.0324\ pu$

C. Wind Turbine-Generator Parameters

$R = 15.72\ m$	$\beta = 0$	$N = 40.65$
$D_l = D_h = 0$	$D_r = 0$	$D_g = 0$
$K_h = 2613.7\ pu$	$K_l = 65.99\ pu$	
$J_g = 0.0329\ pu.s^2$	$J_r = 0.9951\ pu.s^2$	
$X_{ls} = 0.6583\ pu$	$X_{lr} = 0.6818\ pu$	$X_M = 27.777\ pu$
$X_{ss} = 28.435\ pu$	$X_{rr} = 28.458\ pu$	
$r_s = 0.2833\ pu$	$r_r = 0.1167\ pu$	

References

[1] S. Heier *Grid Integration of Wind Energy Conversion Systems*, Wiley Publishing Inc., 1998.

[2] W. E. Leithead, M. C. M. Rogers, *Drive-train Characteristics of Constant Speed HAWT's: Part I- Representation by Simple Dynamic Models*, Wind Engineering, Vol. 20, No. 3, pp. 149-174, 1996

[3] J. Wilkie, W. E. Leithead, C. Anderson, *Modelling of Wind Turbines by Simple Models*, Wind Engineering, Vol. 14, No. 4, pp. 247-274, 1990

[4] N. Bao, Z. Ye, *Active Pitch Control in Larger Scale Fixed Speed Horizantal Axis Wind Turbine Systems Part I: Linear Controller Design*, Wind Engineering, Vol. 25, No. 6, pp. 339-351, 2001

[5] P. C. Krause, D. Wasynczuk, S. D. Sudhoff, *Analysis of Electric Machinery*, IEEE Press, 1995.

[6] S. K. Salman, A. L. J. Teo, *Windmill modeling consideration and factors influencing the stability of a grid-connected wind power-based embedded generator*, IEEE Trans. on Power Systems, Vol. 18, No. 2, pp. 793-802, May 2003.

Ahmadreza Tabesh (Student Member-01) was born in Isfahan, Iran. He received his B.Sc. in electronics and M.Sc. in control systems from Isfahan University of Technology (IUT), Iran, in 1995 and 1998, respectively. He was a faculty member of IUT in the Submarine R&D Center from 1998 to 2001 when he joined the Department of Electrical Engineering at University of Toronto as a Ph.D. student. His research interests include applications of control theory to power systems and power electronics.

Reza Iravani (M-85, SM-00, F-03) received his B.Sc. in electrical engineering in 1976 from Tehran Polytechnique University, Iran. He worked as consulting engineer from 1976 to 1979. He received his M.Sc. and Ph.D degrees also in electrical engineering from the University of Manitoba, Canada, in 1981 and 1985 respectively. He is a professor at the University of Toronto. His research interests include power system dynamics and power electronics.